Flow field characterisation of aggregating human blood in bifurcating microchannels

Joseph M. SHERWOOD[1*], Jonathan DUSTING[2], Efstathios KALIVIOTIS[1], Stavroula BALABANI[3]

* Corresponding author: Tel.: +44 (0)207 848 2902; Email: joseph.sherwood@kcl.ac.uk
1: Division of Engineering, Kings College London, UK
2: Department of Chemistry, Imperial College London, UK
3: Department of Mechanical Engineering, University College London, UK

Abstract Erythrocyte aggregation is a shear dependent physiological phenomenon that modifies local properties of blood flow. Blood flow characteristics in microvascular bifurcations are dependent on many parameters; however the influence of erythrocyte aggregation has not been investigated previously *in vitro*. In the present study, micro-PIV is used to provide high spatial resolution velocity data for both erythrocytes and suspending medium for aggregating and non-aggregating human blood samples in a microchannel with a T-bifurcation geometry on the scale of the microcirculation. Simultaneous hematocrit distributions are inferred from brightfield images. Full field shear distributions are described for an evenly split flow and single flow rate. Velocity profiles of cells upstream of the bifurcation are found to be less blunt than those of the suspended particles. Daughter branch velocity profiles downstream of the bifurcation are skewed towards the wall closest to the parent branch, and non-aggregating cell velocities are significantly less blunted than those of the aggregating case. The local hematocrit is increased at the channel wall opposite the parent branch and a cell-depleted layer is observed near the channel wall closest to the parent branch. Thus, it is shown that aggregation influences both hematocrit and velocity distributions around and downstream of a bifurcation.

Keywords: Microchannel, Blood, Aggregation, Bifurcation, PIV

1. Introduction

Altered blood flow characteristics have been found to be complicit in a large number of pathological conditions, and thus improving understanding of the rheological properties of blood flow is of great importance. Blood can be considered as a two phase fluid consisting of deformable cells suspended in a continuous fluid phase. As the dimensions of the geometry in which the blood flows approaches the scale of the cells, the fluid exhibits an increasingly shear thinning behaviour, which has been attributed to the deformation and aggregation of the erythrocytes (red blood cells). The widely accepted depletion model of erythrocyte aggregation attributes the phenomenon to an attraction between cells, caused by an osmotic gradient due to a depletion of plasma proteins in the region close to the cell (Meiselman 2009). The cells tend to join face to face, forming rouleaux and subsequently clumps or networks. Disaggregation occurs as a result of shear forces acting on the aggregates. While aggregation locally increases the viscosity of the blood, it can also enhance axial migration of the cells (and aggregates), increasing the size of the low viscosity, cell-depleted layer near the wall (Reinke et al. 1986). As a result, aggregation can have different effects on the flow resistance, depending on a number of parameters. Aggregation has been shown to generally increase flow resistance *in vivo* (Bishop et al. 2001) while decreasing flow resistance in channel flow *in vitro* (Reinke et al 1986). This incongruity, along with the question of whether aggregation is physiologically beneficial, is still to be resolved.

The distribution of cells in microvascular bifurcations is of importance as it affects the

delivery of erythrocytes into the capillary bed and thus impacts upon oxygen delivery. Previous studies have shown that a disproportionately large number of cells tend to enter the high flow rate branch, decreasing the hematocrit in the low flow rate branch in a process known as plasma skimming. Feed hematocrit and flow ratio between the outlet branches have been found to be the key parameters (Fenton et al. 1985, Pries et al. 1989), whereas parent vessel flow rate, diameter ratio and branching angle are less significant (Barber et al. 2008, Carr and Wickham 1991). However, aggregation has not generally been considered, with the exception of Chesnutt and Marshall (2009), who simulated the flow in a bifurcation and found that, as particles follow fluid streamlines, aggregation does not affect plasma skimming, although this has not been confirmed by experimental data. Velocities in the microcirculation range between 0.2 and 10 *mm/s* (Fung, 1997), are proportional to vessel diameter and are relatively higher on the arterial side of the capillary bed, where bifurcations are found. Although the flow rates found in arterioles are generally high enough to prevent aggregation, under reduced flow conditions, such as can occur in pathological conditions, shear rates may be sufficiently low to allow aggregation. Ong et al. (2010) reported on the effect of aggregation on cell-free layer formation in arterioles under reduced flow conditions. There are few studies on the influence of aggregation on the flow in and around microvascular bifurcations reported in the literature. Many previous experimental studies have only considered bulk measurements (Fenton et al. 1985) or qualitative descriptions of the flow around the bifurcation. While, some have considered Lagrangian descriptions based on tracking fluoresced erythrocytes (Ishikawa et al. 2011), detailed full-field flow information has not been reported.

Particle Image Velocimetry (PIV) is a non-invasive velocity measurement technique involving correlation of pairs of particle images. Micro-PIV has been previously used to measure blood flow both *in vitro* and *in vivo* using either images of erythrocytes or fluorescent particles seeded in the flow (e.g. Dusting et al. 2009, Lima et al. 2008, Vennemann et al. 2006).

In the present study, both erythrocytes and tracer particles are used for PIV measurements in order to establish the influence of aggregation on the flow of both the cells and the suspending medium in a bifurcating geometry on the scale of the microcirculation.

2. Materials and Methods

The study was approved by the South East London Research Ethics Committee (ref:10/H0804/21). Blood samples were acquired from healthy volunteers into vacuum tubes (BD, 367873) containing 1.8 mg/ml EDTA to prevent coagulation. The erythrocytes were separated from the plasma via centrifugation at 3600 *rpm* for 5 minutes then washed twice in Phosphate Buffered Saline (PBS) in the same manner. Finally, they were re-suspended in PBS at a volume concentration (hematocrit) of 25%. For the aggregating cases Dextran 2000 at a concentration of $5\text{x}10^{-3}$ *kg/L* was added to the suspending medium. Additionally, for the PIV cases, 1.1μm diameter fluorescent rhodamine particles (Invitrogen, USA) were added at a volume concentration of 0.1%.

A PDMS microchannel (Epigem, UK) with a cross section of 100x40μm was employed, featuring a T-junction after a straight channel section of 40 *mm.* The channel was mounted on the stage of an inverted microscope (Leica, Germany), as shown in figure 1a, and the focal plane was positioned at the centre of the channel.

The working fluid was placed in a sealed inlet reservoir and continuously mixed using a magnetic stir bar in order to minimize the effects of aggregation and sedimentation in the inlet reservoir and feed tubing. The inlet reservoir was connected to a compressed nitrogen cylinder and the pressure controlled using a needle valve actuated with a stepper motor and monitored using a pressure gauge. A leak valve was included in the pressure system in order to improve the temporal response to a drop in pressure. The fluid was

infused through the microchannel via PTFE tubing of 0.5*mm* ID and the flow rate controlled by varying the pressure in the inlet reservoir. The outlets of the T-junction were connected to two outlet reservoirs mounted on micrometer stages which allowed the flow ratio between the branches to be changed.

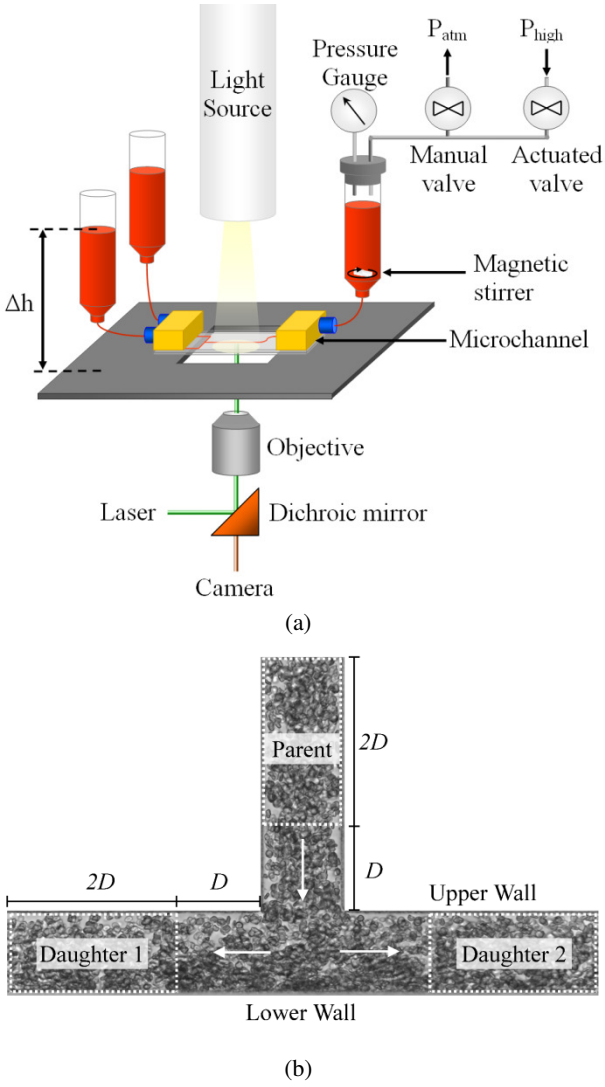

Figure 1 – (a) Schematic of the experimental setup (b) Typical brightfield image of aggregating blood showing the branch names, regions of analysis used for velocity profiles (dashed lines) and flow directions (arrows). *D* is the channel width

For the cell velocity data, the channel was illuminated using a 100*W* halogen light source and images were acquired with an IDT X3 CMOS camera (IDT, USA) at 500Hz for 5 seconds. For the suspending medium velocity data, the fluorescent particles seeded in the flow were illuminated with a dual cavity Nd:Yag laser (532nm) (New Wave, USA) and the fluoresced light was passed through a dichroic mirror with a wavelength of 610 nm and 75*nm* bandwidth. Images were acquired with a Hamamatsu C8484-05C CCD (Hamamatsu, Japan) camera in double frame mode at 5Hz for 20 seconds. In order to ensure the cell distribution in the channel was uniform, alternate brightfield frames were acquired using a microstrobe (Dantec Dynamics, Denmark) focused using plano-convex lenses and positioned with an XY micrometer stage. The strobe was triggered in the second frame of the double frame acquisition and the first frame was discarded. A 20*x* objective was used with the CMOS camera and a 10*x* objective with the CCD camera, resulting in similar pixel pitch values between the two data sets. The flow and timing control and image acquisition were carried out using LabVIEW (National Instruments).

Prior to each acquisition, the pressure was maintained at a high value to ensure all cells in the flow system were disaggregated and the hematocrit was uniform. It was then decreased to the target value over a period of 5 seconds. Image acquisition was triggered 20 seconds later, so that flow rates and aggregation had reached a steady state.

The acquired images were pre-processed in order to ensure that the PIV interrogation windows were suitably aligned with the channel images. The images were scaled down using cubic spline interpolation, so that interrogation windows of 16 pixels would fit evenly within the channel. The final channel width was 136 pixels for both cell and particle images, giving a resolution of 0.74 *μm/pixel*. The images were then cropped to be 7*D* wide and 4*D* high, where *D* is the channel width, as shown in figure 1b. For the particle images, the background, calculated from the minimum intensity at each pixel, was subtracted.

PIV processing was carried out using the software package JPIV (www.jpiv.vennemann-online.de). Three passes were used with a final interrogation window of 16 pixels and a vector spacing of 8 pixels. Ensemble correlations of 50 image pairs were used. The average parent branch velocities calculated using instantaneous vector fields had root-mean-square values of approximately 1% for cell

images and 0.5% for particle images, thus time averaging is a suitable approach. Vector fields were post-processed using a normalised median test and invalid vectors were replaced by the median of the surrounding vectors.
Due to optical limitations, a region of about 4 pixels next to each channel wall was excluded from the PIV analysis. Thus, the first velocity vector that could be accurately calculated from the PIV images was 12 pixels from the wall. Using cubic spline interpolation between 4 successive vectors in the transverse direction, and assuming a no-slip condition, a vector closer to the wall (4 pixels) was estimated. This approach was used in order to avoid the assumption of a linear velocity profile near the wall when calculating average velocities.

3. Results and Discussion

Four cases are considered in the present study: aggregating and non-aggregating fluids with velocity data obtained from both cells and seeded particles (suspending medium). To limit the parameter space, the parent branch velocities and flow ratios were matched as closely as possible. As the flow rate was not measured in the study, the flow ratio between the parent branch and one of the daughter branches was determined from the ratio of average velocities, $Q^*=V_p/V_{d1}$, where V_p and V_{d1} are the average velocities in the parent and daughter branch 1 respectively, as indicated in figure 1b. In order to ascertain that this is a reasonable assumption, especially given the altered flow profiles expected, the error in continuity was calculated according to $e_c=(V_p - V_{d1} - V_{d2})/V_p$. The error values are listed in table 1, together with parent branch velocities and flow ratios for the four cases tested.

Table 1 – Summary of parameters for each case

Case	V_p (mm/s)	Q^*(%)	e_c(%)
Aggregating, Cells	0.57	48	3.4
Aggregating, Particles	0.61	50	1.0
Non-Aggregating, Cells	0.53	53	1.0
Non-Aggregating, Particles	0.59	49	4.3

It can be seen that the continuity error is 1% and less than 5% for suspending medium and cell velocities respectively. Furthermore, the flow ratio, Q^* is within 3% of that for an evenly split flow. Despite the slight variation in the parent branch velocities for the four cases tested, their effect on the results is expected to be insignificant on the basis of past evidence (Fenton et al. 1985).
Based on the theoretical solution for a Newtonian fluid in a rectangular channel, the average velocity in the centre plane is around 1.5 times the average velocity of the entire flow field. Accordingly, the flow rate can be estimated to be approximately 5 $\mu l/hour$ and the Reynolds number, based on hydraulic diameter and physical properties of the suspending medium, is of the order of $5x10^{-3}$. It should be noted that the viscosity is dependent on aggregation and local hematocrit, which leads to spatial variation of Re within the flow domain. Furthermore, the addition of Dextran to the suspending medium increases its viscosity by ~30%. Nonetheless, the resulting Reynolds number range will be similar and viscous forces will dominate.
The feed branch hematocrit was 25%. However, due to the Fåhraeus effect, the channel hematocrit is expected to be reduced. According to the data acquired by Barbee and Cokelet (1971) and based on the hydraulic diameter, this can be approximated to 17.5% for the present data.

3.1 Flow around the bifurcation

Figure 2 shows brightfield images of aggregating and non-aggregating blood in the bifurcation. In figure 2a, individual cells and rouleaux can be clearly seen and there are many visible gaps where no cells are present, particularly near the parent branch and daughter branch upper walls. Furthermore, the images are darker along the lower wall, where the local hematocrit is increased as the cells and aggregates reduce in velocity around the stagnation point. For the non-aggregating case in figure 2b, the cells are more uniformly distributed throughout the channel. Similar distributions in intensity around the walls can be observed, but of significantly lower magnitude. This distribution is discussed in further detail below.

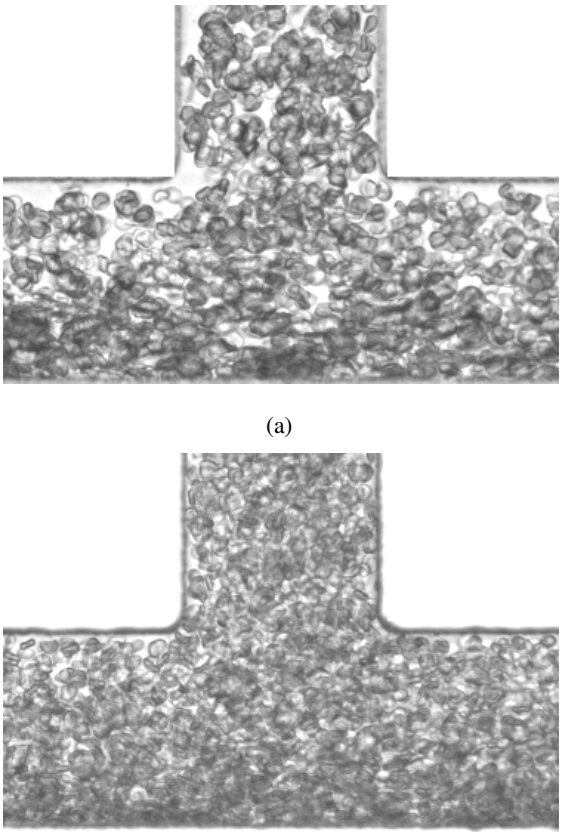

(a)

(b)

Figure 2 – Brightfield image of (a) aggregating and (b) non-aggregating blood in the region of the bifurcation. Brightness and contrast have been increased by 10% for clarity

Figure 3a shows suspending medium velocity vectors in the region of the bifurcation for the aggregating case. Only every other vector in both directions is shown for clarity. It can be seen that the velocity profile is in the parent branch, but is skewed towards the upper wall in the daughter branches.

Figure 3b shows the in-plane shear rates calculated from the vector field for the same case, using a central differencing scheme. In the centre of the parent branch the shear rates are very low, with higher shear rates at the walls, particularly in the parent branch. As aggregation is shear dependent, the shear rate values and distribution observed in Figure 3b suggest that the aggregation characteristics will vary throughout the bifurcation.

It should be noted, however, that due to the high channel aspect ratio employed in the present study, the out of plane shear values may also be significant, and in some regions exceed the in-plane shear values.

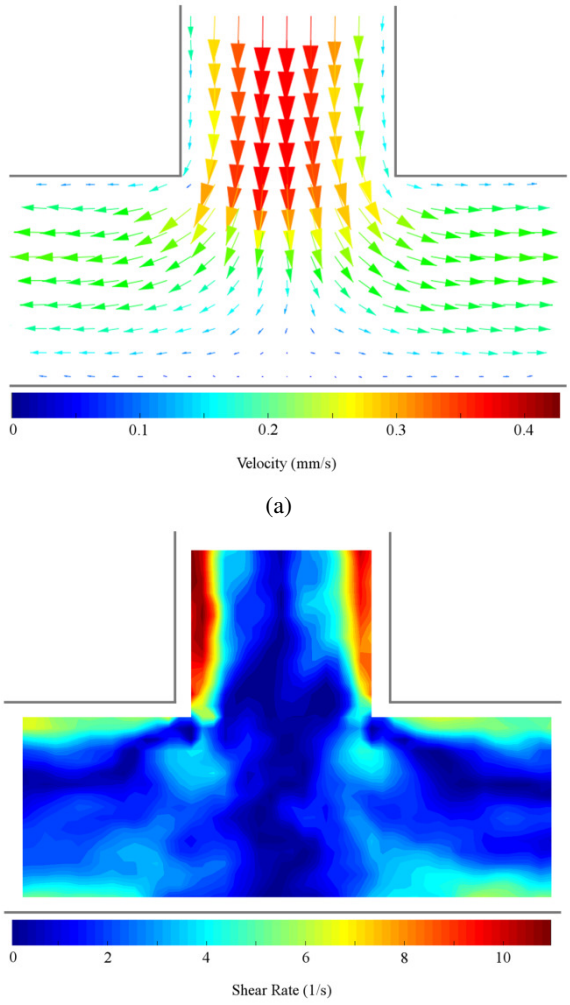

(a)

(b)

Figure 3 – (a) Velocity vectors and (b) in-plane shear rates in the region of the bifurcation for the aggregating case

3.2 Parent branch velocity profiles

Velocity profiles were calculated by averaging along the parent branch over a distance of $2D$ as indicated in figure 1b. In these regions, the velocity component perpendicular to the direction of the flow was negligible (<2%). Each point shown is thus the average of 34 vectors and error bars show the standard deviation. Data were fitted according to the standard blunted profile equation.

$$V = V_{\max}\left(1-\left(\frac{r}{R}\right)^{k}\right) \qquad (1)$$

Where k is a bluntness parameter, and is equal to 2 for a parabolic profile. While equation 1 is not directly applicable to the velocity profile in a channel of rectangular cross-section, the

calculated k values give an indication of the bluntness. Calculated values, listed in table 2, were found to give a mean residual of less than 3%.

Table 2 – Bluntness parameter k for parent profiles

	Cells	Particles
Aggregating	2.76	3.34
Non-aggregating	2.65	3.26

It can be seen that the suspending medium velocity profiles are significantly blunter than those of the cells for both aggregating and non-aggregating cases.

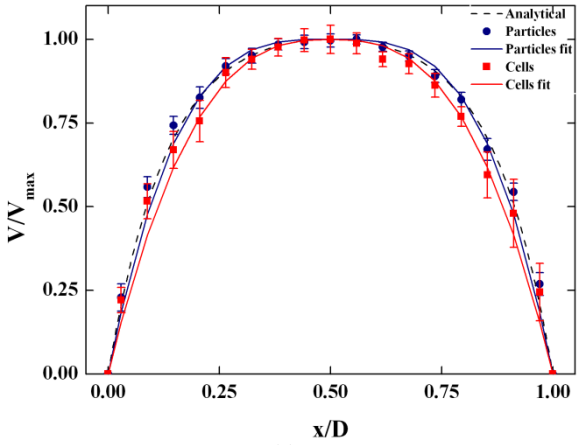

(a)

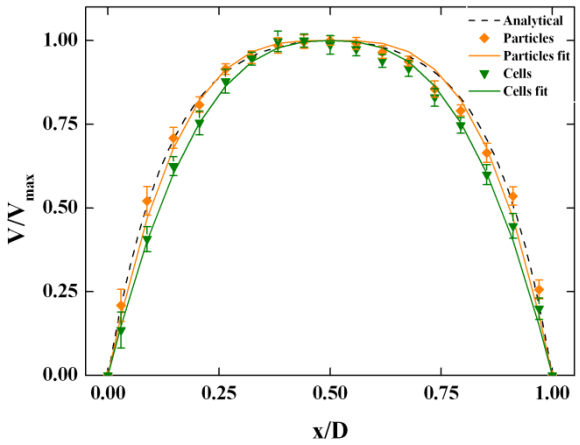

(b)

Figure 4 – Parent branch velocity profiles for suspending medium and cells for (a) aggregating and (b) non-aggregating cases

This can be seen in figure 4a and 4b respectively, where the points represent experimental data and lines show the empirical fits according to equation 1. Velocities are normalised with maximum value and x/D represents the normalised distance from the channel wall. In addition, the results are compared with the analytical solution for a Newtonian fluid (Bruus, 2008), as indicated by the grey line in figures 4 and 5. For the analytical solution, k=3.46, i.e. the geometry results in a blunted profile for a Newtonian fluid. As the erythrocytes axially migrate, their velocity is higher, an effect which leads to a reduction in tube hematocrit known as the Fåhraeus effect. This explains why their profiles are less blunt than those of the suspending medium. It can also be seen from table 2 that the velocity profiles of both suspending medium and cells are slightly more blunted for the aggregating case. This is a result of the increased axial migration of aggregating blood as described by Reinke et al. (1986). For both the aggregating and non-aggregating cases, the velocity profile of the suspending medium is not significantly different to the analytical solution for a Newtonian fluid.

3.3 Daughter branch velocity profiles

Daughter branch velocity profiles were calculated by averaging along the daughter channels over a distance of 2D as indicated by the region labelled ‘daughter 1’ in figure 1b. Within this region, the radial position and magnitude of the maximum velocity did not measurably change.

For all cases, the maximum velocity in the daughter branch was located approximately 0.1D from the centreline towards the upper wall. Due to axial migration in the parent branch, the local hematocrit is higher in the channel centre, and thus as the cells move through the bifurcation, there will be an increased distribution towards the lower wall. This will increase local viscosity, and thus resistance to flow, resulting in the skewed velocity profiles observed in the daughter branches.

Figure 5a compares the daughter branch cell velocity profiles, where x/D=0 corresponds to the upper wall. The lines represent Bezier-spline fits to aid visualisation and only the profiles from the daughter branch 1 are shown for clarity. Distributions in daughter branch 2 were similar. It can be seen that while the velocity profile for the aggregated case is blunt,

the non-aggregating one is relatively sharp. The suspending media profiles shown in figure 5b are found to have blunt profiles, for both aggregating and non-aggregating cases, not significantly different from that for the aggregated cell profiles. There is a marked difference for all cases compared to the analytical solution for a Newtonian fluid.

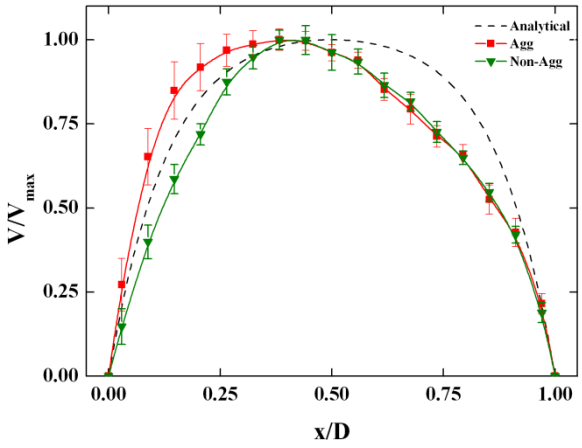

(a)

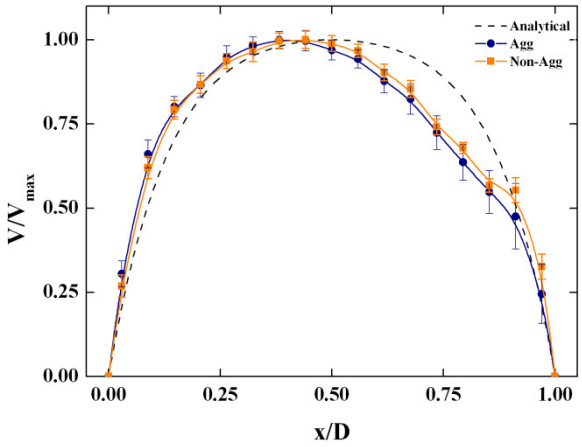

(b)

Figure 5 – Daughter branch velocity profiles for (a) cells and (b) suspending medium

The disparity between the degree of blunting between the aggregating and non-aggregating cell velocities can be attributed to the tendency of rouleaux and clumps, which can be seen in figure 2a, to blunt velocity profiles. This increased blunting results in an increased shear on the upper channel wall.

3.4 Hematocrit distribution

The intensities of the image at each pixel can provide information on hematocrit distribution and thus also the cell-depleted layer, if one exists. For a given pixel, the average intensity value gives time averaged information on the number of cells that have passed through that point in the flow. The background pixel intensities are distributed within a small range of high values. Conversely, the presence of cells at a given pixel results in a relatively normal distribution with a lower mean value. Therefore, the intensity distribution for a single pixel is skewed towards high values for regions where there are often no cells. As a result, the median intensity value is more sensitive than the mean as a measure of cell depletion near the wall, and is thus utilised herein. Figure 6 shows the time averaged median pixel values over 2500 images in the region around the bifurcation for aggregating and non-aggregating cases.

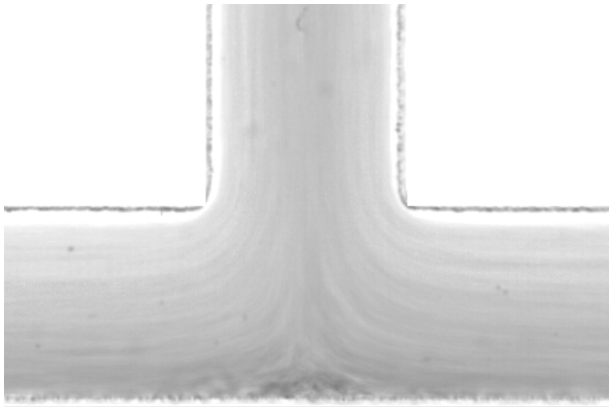

(a)

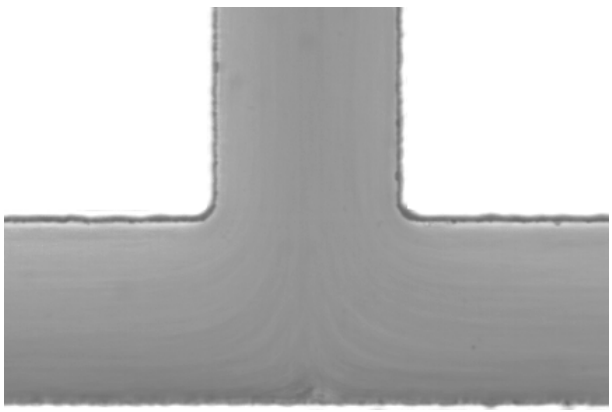

(b)

Figure 6 – Median intensity images for (a) aggregating and (b) non-aggregating cases. Brightness has been increased by 10% for clarity

For the parent branch, a wide cell-depleted layer is apparent for the aggregating case, but not for the non-aggregating case. This is consistent with previous reports of enhanced cell-depleted layer formation as a result of

aggregation (Reinke et al. 1986). A cell-depleted layer is also observed at the upper wall of the daughter branches. For the non-aggregating case, this layer is very thin. Aggregation is seen to greatly enhance the layer, with the width increasing in the direction of the flow in the vicinity of the vertices. It should be noted that these low cell density regions will result in decreased local viscosity, which will counteract the increased wall shear occurring due to the blunted cell velocity profiles.

The increased hematocrit at the lower wall discussed earlier can be observed in both cases. The latter can explain the skewed velocity profiles further downstream (figure 5), as the increased local hematocrit will increase viscosity and thus flow resistance with proximity to the lower wall.

4. Conclusion

Although there is a large number of studies on bifurcating geometries *in vitro* and *in vivo*, high resolution experimental velocity and erythrocyte distribution data has not, to the authors' knowledge, been previously reported and aggregation has generally been excluded from the parameter space. Particularly for aggregating blood, whose viscosity is highly shear dependent, the need for high resolution data is exemplified by the fact that in general, a pseudoshear rate, $\gamma=V_{av}/D$, is generally reported in the literature. For the present study this value is approximately $6s^{-1}$. Although this is a reasonable approximation of the average value, the present study shows that the shear distribution should be taken into account.

Despite the fact that the high aspect ratio of the channel used in the study may attenuate the effects of aggregation, the present data has clearly demonstrated modifications of both velocity and hematocrit distributions within, and downstream of the bifurcation. Given the complexity of the microvasculature in terms of both flow and geometric parameters, and the demonstrated influence of aggregation, further experimentation is required to fully elucidate its impact on microcirculatory phenomena, such as plasma skimming and leukocyte margination.

5. References

Barber, J.O., Alberding, J.P., Restrepo, J.M. and Secomb, T.W., 2008. Simulated two-dimensional red blood cell motion, deformation, and partitioning in microvessel bifurcations. *Ann. of Biomed. Eng*., 36,10:1690–1698.

Bishop, J.J., Nance, P.R., Popel, A.S., Intaglietta, M. and Johnson, P.C., 2001. Effect of erythrocyte aggregation on velocity profiles in venules. *Am. J. Phys.: Heart and Circ. Phys.* 280:H222–H236.

Bruus, H., 2008. Theoretical microfluidics. *Oxford university press.*

Carr, R.T. and Wickham, L.L., 1991. Influence of vessel diameter on red cell distribution at microvascular bifurcations. *Microvascular Res.*, 41:184–196.

Chesnutt, J.K.W. and Marshall. J.S. 2009. Effect of particle collisions and aggregation on red blood cell passage through a bifurcation. *Microvascular Res.*, 78:301–313.

Dusting, J., Kaliviotis, E., Balabani, S. and Yianneskis, M. 2009. Coupled human erythrocyte velocity field and aggregation measurements at physiological haematocrit levels. *J. Biomechanics*, 42:1438–1443.

Fenton, B.M., Carr, R.T. and Cokelet, G.R., 1985. Nonuniform red cell distribution in 20 to 100 um bifurcations. *Microvascular Res.*, 29:103–126.

Fung, Y., 1997. Biomechanics: Circulation. 2nd edition. *Springer.*

Ishikawa, T., Fujiwara, H., Matsuki, N., Yoshimoto, T., Imai, Y., Ueno, H. And Yamaguchi,T., 2011. Asymmetry of blood flow and cancer cell adhesion in a microchannel with symmetric bifurcation and confluence *Biomed. Microdevices.* 13:159–167.

Lima, R., Wada, S.,Tanaka, S., Takeda, M., Ishikawa, T., Tsubota, K., Imai, Y. and Yamaguchi, T., 2008. *In vitro* blood flow in a rectangular PDMS microchannel: experimental observations using a confocal micro-PIV system. *Biomed. Microdevices*, 10:153–167.

Meiselman, H., 2009. Red blood cell aggregation: 45 years being curious. *Biorheology.* 46:1–19.

Ong, P.K., Namgung, B., Johnson, P.C., and Kim, S. 2010. Effect of erythrocyte aggregation and flow rate on cell-free layer formation in arterioles. *Am. J. Phys.: Heart and Circ. Phys.* 298:1870-1878.

Pries A.R., Ley, K., Claasen, M. Gaehtgens, P., 1989. Red cell distribution at microvascular bifurcations. *Microvascular Res.* 38:81-101.

Reinke, W., Johnson, P.C. and Gaehtgens, P. 1986. Effect of shear rate variation on apparent viscosity of human blood in tubes of 29 to 94 μm diameter. *Circ. Res.*, 59, No. 2:124–132.

Vennemann, P., Kiger, K., Lindken, R., Groenendijk, B., Stekelenburg-de Vos, S., ten Hagen, T., Ursem, N., Poelmann, R.,Westerweel, J., Hierck, B., 2006. *In vivo* micro particle image velocimetry measurements of blood-plasma in the embryonic avian heart. *Journal of Biomechanics* 39:1191–1200.